

THE MAGNETIC HELICITY INJECTED BY SHEARING MOTIONS

P. DÉMOULIN¹, C. H. MANDRINI^{2,*}, L. VAN DRIEL-GESZTELYI^{1,3,4,5},
M. C. LOPEZ FUENTES² and G. AULANIER¹

¹*Observatoire de Paris, section Meudon, DASOP, URA 2080 (CNRS), F-92195 Meudon Principal
Cedex, France, (e-mail: pascal.demoulin@obspm.fr)*

²*Instituto de Astronomía y Física del Espacio, IAFE, CC. 67 Suc. 28, 1428 Buenos Aires,
Argentina, (e-mail: mandrini@iafe.uba.ar)*

³*Mullard Space Science Laboratory, University College London, U.K.*

⁴*Konkoly Observatory, Hungary*

⁵*Centre for Plasma Astrophysics, K.U. Leuven, Celestijnenlaan 200B, 3001 Heverlee, Belgium*

(Received 19 September 2001; accepted 4 December 2001)

Abstract. Photospheric shearing motions are one of the possible ways to inject magnetic helicity into the corona. We explore their efficiency as a function of their particular properties and those of the magnetic field configuration. Based on the work of M. A. Berger, we separate the helicity injection into two terms: twist and writhe. For shearing motions concentrated between the centers of two magnetic polarities the helicity injected by twist and writhe add up, while for spatially more extended shearing motions, such as differential rotation, twist and writhe helicity have opposite signs and partially cancel. This implies that the amount of injected helicity can change in sign with time even if the shear velocity is time independent. We confirm the amount of helicity injected by differential rotation in a bipole in the two particular cases studied by DeVore (2000), and further explore the parameter space on which this injection depends. For a given latitude, tilt and magnetic flux, the generation of helicity is slightly more efficient in young active regions than in decayed ones (up to a factor 2). The helicity injection is mostly affected by the tilt of the AR with respect to the solar equator. The total helicity injected by shearing motions, with both spatial and temporal coherence, is at most equivalent to that of a twisted flux tube having the same magnetic flux and a number of turns of 0.3. In the solar case, where the motions have not such global coherence, the injection of helicity is expected to be much smaller, while for differential rotation this maximum value reduces to 0.2 turns. We conclude that shearing motions are a relatively inefficient way to bring magnetic helicity into the corona (compared to the helicity carried by a significantly twisted flux tube).

1. Introduction

Magnetic helicity plays a key role in magnetohydrodynamics (MHD) because it is one of the few global quantities which are preserved (see, e.g., Biskamp, 1993, Chapter 7). Helicity is conserved not only in ideal MHD, but also in resistive MHD on time scales shorter than the global diffusion time scale (Berger, 1984). For solar plasmas this diffusion time scale is several orders of magnitude larger than the relevant time scale for the evolution of magnetic fields, e.g., for a typical coronal loop, Berger (1984) found a minimum helicity dissipation time of the order of

*Member of the Carrera del Investigador Científico, CONICET, Argentina.



Solar Physics **207**: 87–110, 2002.

© 2002 Kluwer Academic Publishers. Printed in the Netherlands.

10^5 years with a classical resistivity (see his Equation (57), this time scale reduces proportionally to the resistivity if it is enhanced over the classical one). Moreover, magnetic helicity is also preserved with a very good approximation during magnetic reconnection. This conservation of magnetic helicity has led to Taylor's theory (Taylor, 1974): the minimum energy state of a magnetic field, preserving magnetic helicity, is a linear (or constant α) force-free field. Conversely compared to magnetic energy, which is efficiently transported to the small spatial scales, magnetic helicity cascades to the large scales. Subsequently, magnetic energy is much more rapidly dissipated (transformed into other forms of energy) than magnetic helicity. The conservation of magnetic helicity gives an important tool for understanding the link between phenomena present in very different physical conditions, such as in the convective zone, the corona and the interplanetary medium.

There are two principal mechanisms (e.g., Seehafer, 1990) through which magnetic helicity can be injected into the solar corona. One of them is through the emergence of twisted magnetic flux tubes from the bottom of the convection zone, where dynamo action amplifies the fields. The second one implies the shearing (or twisting) of magnetic fields by large-scale photospheric motions, like the differential rotation. Evidence for the first mechanism is the observation of chirality patterns in young active regions (e.g., Seehafer, 1990; Pevtsov, Canfield, and Metcalf, 1995), and the inference of strong electric currents in newly emerged flux (Leka *et al.*, 1996; Wang, 1996). Shearing motions have been widely used in MHD numerical simulations (e.g., Mikić and Linker, 1994; DeVore and Antiochos, 2000). In particular, differential rotation is injecting helicity in ARs (DeVore, 2000).

The definition and the computation of the relative magnetic helicity is recalled in Section 2.1. The injection of magnetic helicity within a volume via boundary motions is summarized in Section 2.2, then the notion of twist and writhe helicity is introduced (Section 2.3). These results are applied to a set of theoretical configurations in the next two sections. In Section 3, we investigate shearing motions which are parallel and concentrated around the photospheric inversion line (PIL) of the magnetic field component normal to photosphere. Section 4 is devoted to a particular shearing motion: differential rotation. Then, in Section 5 we compare the amounts of helicity injected by shearing motions to those contained in twisted magnetic configurations. Finally, in Section 6, we discuss our findings. We conclude that shearing motions, in particular differential rotation, are not efficient processes to inject magnetic helicity into the coronal field.

2. Magnetic Helicity

2.1. DEFINITION OF THE RELATIVE MAGNETIC HELICITY

The magnetic helicity of a field \mathbf{B} within a volume V is defined by

$$H = \int_V \mathbf{A} \cdot \mathbf{B} \, dV, \quad (1)$$

where the vector potential \mathbf{A} satisfies

$$\mathbf{B} = \nabla \times \mathbf{A}. \quad (2)$$

However, Equation (1) is physically meaningful only when the magnetic field is fully contained inside the volume V (i.e., at any point of the surface S surrounding V , the normal component $B_n = \mathbf{B} \cdot \hat{n}$ vanishes); this is because the vector potential is defined only up to a gauge transformation ($\mathbf{A}' = \mathbf{A} + \nabla\Phi$), then H is gauge-invariant only when $B_n = 0$.

Berger and Field (1984) have shown that for cases where $B_n \neq 0$ one can define a relative magnetic helicity (H_r) subtracting the helicity of a reference field \mathbf{B}_0 , having the same distribution of B_n on S :

$$H_r = \int_V \mathbf{A} \cdot \mathbf{B} \, dV - \int_V \mathbf{A}_0 \cdot \mathbf{B}_0 \, dV. \quad (3)$$

Berger and Field (1984) and Finn and Antonsen (1985) have shown that H_r is gauge-invariant, and that H_r does not depend on the common extension of \mathbf{B} and \mathbf{B}_0 outside V . A convenient choice for the reference field \mathbf{B}_0 is a potential field with \mathbf{A}_0 satisfying Equation (2), $\nabla \cdot \mathbf{A}_0 = 0$ and $(A_0)_n = 0$ on S ; in this way the helicity $\int_V \mathbf{A}_0 \cdot \mathbf{B}_0 \, dV$ vanishes (Berger, 1988).

2.2. INJECTION OF MAGNETIC HELICITY

Since H_r is well preserved under solar conditions (see Introduction), the only way helicity can be modified inside V is because of helicity flux crossing the boundary S (S being the photospheric boundary in our case). The change of relative helicity is (Berger and Field, 1984):

$$\frac{dH_r}{dt} = -2 \int_S [(\mathbf{A}_0 \cdot \mathbf{v})\mathbf{B} - (\mathbf{A}_0 \cdot \mathbf{B})\mathbf{v}] \cdot d\mathbf{S}, \quad (4)$$

where \mathbf{v} is the velocity of the plasma. The last term on the right-hand side of Equation (4) represents a direct ‘inflow’ of plasma inside the volume V (for $\mathbf{v} \cdot d\mathbf{S} > 0$, otherwise ‘inflow’ should be replaced by ‘outflow’), which carries magnetic helicity together with the magnetic flux. In order to evaluate the amount of H_r injected by shearing motions, we only have to consider the first term on the right-hand side of Equation (4). This term represents the injection of helicity by plasma motions parallel to the surface S . In this case, Equation (4) reduces to

$$\frac{dH_r}{dt} = -2 \int_S (\mathbf{A}_0 \cdot \mathbf{v}) B_n dS. \quad (5)$$

This helicity injection depends only on plasma motions \mathbf{v} and the normal field B_n , integrated over all positions \mathbf{r} on S ; being so because \mathbf{A}_0 for the potential field \mathbf{B}_0 can be expressed only as a function of B_n on S . This contrasts with the injection of energy (Poynting flux), which also depends on the stress of the field into the corona. In this way, we can compute the injection of magnetic helicity without computing explicitly the evolution of the magnetic field in V (i.e., the corona) by solving numerically the MHD equations.

For simplicity, let us assume that the photosphere is locally planar at the scale size of an AR (see Berger and Ruzmaikin, 2000, for a spherical version). Computing \mathbf{A}_0 as a function of the B_n distribution, Berger (1984, 1988) derived an expression for dH_r/dt that depends only on observable photospheric quantities (B_n , \mathbf{R} and \mathbf{v}):

$$\frac{dH_r}{dt} = -\frac{1}{\pi} \int_S \int_{S'} \frac{\mathbf{R} \times \mathbf{v}(\mathbf{r})}{R^2} \Big|_n B_n(\mathbf{r}) B_n(\mathbf{r}') dS dS', \quad (6)$$

where $\mathbf{R} = \mathbf{r} - \mathbf{r}'$ is the difference between two spatial positions on the photospheric plane. This equation involves a double integration on the boundary. Since the integrations are done on the same surfaces, $S = S'$, we can exchange \mathbf{r} and \mathbf{r}' . This yields a new equation that summed up with Equation (6) gives

$$2 \frac{dH_r}{dt} = -\frac{1}{\pi} \int_S \int_{S'} \frac{\mathbf{R} \times [\mathbf{v}(\mathbf{r}) - \mathbf{v}(\mathbf{r}')] }{R^2} \Big|_n B_n(\mathbf{r}) B_n(\mathbf{r}') dS dS'. \quad (7)$$

Let us define θ as the angle between \mathbf{R} and a fixed direction (e.g., the east–west direction) with trigonometric convention (counterclockwise), then:

$$\frac{d\theta}{dt} = \frac{\mathbf{R} \times d\mathbf{R}/dt}{R^2} \Big|_n \quad (8)$$

(with $d\mathbf{R}/dt = \mathbf{v}(\mathbf{r}) - \mathbf{v}(\mathbf{r}')$) and Equation (7) is transformed to

$$\frac{dH_r}{dt} = -\frac{1}{2\pi} \int_S \int_{S'} \frac{d\theta}{dt} B_n(\mathbf{r}) B_n(\mathbf{r}') dS dS'. \quad (9)$$

This equation shows that the helicity injection rate can be understood as the summation of the rotation rate of all the pairs of elementary fluxes weighted with their magnetic flux (as first derived by Berger, 1986).

We stress again that throughout our analysis we are computing the input of helicity only due to horizontal flows; here, we are further supposing that the magnetic flux is not removed from the photosphere (e.g., by magnetic reconnection). Then, the elementary fluxes $B_n(\mathbf{r}) dS$ are time-independent (though they can still change in shape or field strength) and Equation (9) can be integrated:

$$\Delta H_r(t) = -\frac{1}{2\pi} \int_S \int_{S'} \Delta\theta(\mathbf{R}, t) B_n(\mathbf{r}) B_n(\mathbf{r}') dS dS', \quad (10)$$

where $\Delta H_r(t) = H_r(t) - H_r(0)$ is the variation of the relative helicity and $\Delta\theta = \theta(t) - \theta(0)$. As Equation (9), Equation (10) gives a geometrical interpretation to the injected helicity.

2.3. TWIST AND WRITHE HELICITY

The magnetic helicity injected by shearing motions can be separated into two terms:

$$\begin{aligned} \Delta H_r(t) &= -\frac{1}{2\pi} \int \int_{B_n B_n' > 0} \Delta\theta B_n B_n' dS dS' + \\ &\quad + \frac{1}{2\pi} \int \int_{B_n B_n' < 0} \Delta\theta |B_n B_n'| dS dS' \\ &= \Delta H_r(t)|_{\text{twist}} + \Delta H_r(t)|_{\text{writhe}}. \end{aligned} \quad (11)$$

The first term corresponds to the generation of helicity by the rotation of each polarity ($B_n(\mathbf{r}) \cdot B_n(\mathbf{r}') > 0$). This helicity is generated in a similar way as twisting motions would do. The last term, with $B_n(\mathbf{r}) \cdot B_n(\mathbf{r}') < 0$, corresponds to the relative rotation of positive and negative polarities. It basically changes the global shape, more precisely the writhe, of the flux tube linking the opposite polarities. The decomposition in twist and writhe helicity injection applies also to the rate of injection, so that Equation (9) becomes

$$\frac{dH_r}{dt}(t) = \left. \frac{dH_r}{dt}(t) \right|_{\text{twist}} + \left. \frac{dH_r}{dt}(t) \right|_{\text{writhe}}. \quad (12)$$

What is the meaning of this decomposition? Let us consider shearing motions which are not evolving with time, so they deform the initial boundary flux distribution in the same systematic way. For a large set of these shearing motions, $\Delta\theta(t)$ has a given sign and is a monotonic function of time, then both terms $\Delta H_r(t)|_{\text{twist}}$ and $\Delta H_r(t)|_{\text{writhe}}$ also have a given sign and are monotonic functions of time. However, both of these properties do not hold for the total helicity injected when the twist and writhe helicity injected have opposite sign. In such a case the decomposition in the twist and writhe terms is useful to understand the non-monotonic behavior and the change in sign with time of the injected helicity, while the shearing motion stays the same.

3. Generation of Magnetic Helicity by Shearing Motions

3.1. CONFIGURATIONS STUDIED

We use a magnetic configuration created by a sub-photospheric horizontal and potential dipole (Figure 1). The magnetic dipole is oriented in the \hat{y} direction in the Cartesian frame (\hat{x}, \hat{y}) . This flux distribution is characterized by the parameters defined below. The magnetic flux is defined by $\Phi = \int_{B_n > 0} B_n dS = \int_{B_n < 0} |B_n| dS$. The mean photospheric position of the polarities is defined as $\mathbf{r}_+ = \int_{B_n > 0} |B_n| \mathbf{r} dS / \Phi$, with a similar expression for \mathbf{r}_- for the negative polarity. The size of the region is simply defined by $\mathbf{S} = |\mathbf{r}_+ - \mathbf{r}_-|$.

As a first example we consider the shearing motion defined by the velocity v_x :

$$\begin{aligned} v_x &= a \sin \pi y / W && \text{when } |y| \leq W, \\ &= 0 && \text{when } |y| > W, \end{aligned} \quad (13)$$

where a is a numerical coefficient and W is the width of the shearing region on both sides of the PIL (located at $x = 0$). Figure 1(b) shows the deformed flux distribution at the time t when the maximum shear amplitude (at) equals the region size (S). Such a shearing motion was applied to the above bipolar configuration to model a magnetic configuration suited to support a prominence (De Vore and Antiochos, 2000).

As a second example we consider the shearing motion:

$$v_x = a \operatorname{sign}(y) \exp(-2|y|/W). \quad (14)$$

This second example implies a shear around the PIL which is larger than in the first example. Indeed v_x , as defined by Equation (14) is discontinuous at $x = 0$. This can be avoided by multiplying the expression on the right hand side by, e.g., $(1 - \exp(-2|y|/V))$, with $V \ll W$ not to modify significantly the large scale flow. Indeed, because the helicity injection involves B_n^2 , which is a very small quantity near the PIL, both shear profiles give a very similar helicity injection. For simplicity, we keep below the motion defined by Equation (14) as an example of a shearing motion with an amplitude which is decreasing with the distance to the PIL.

3.2. LOCALIZED SHEARING MOTIONS

We analyze below shearing motions localized around the PIL ($W \ll S$), one example is shown in Figure 1(b). For small values of W/S twist and writhe helicity are nearly the same, so the magnetic helicity is a monotonic function of the amplitude of the shear distance. This is still the case for $W/S = 0.2$ (Figure 2(a)). This case is close to the one studied by DeVore and Antiochos (2000) and we find a similar input of magnetic helicity (compare to their Figure 5) when the same normalization is used (we are expressing the helicity in its natural units, Φ^2).

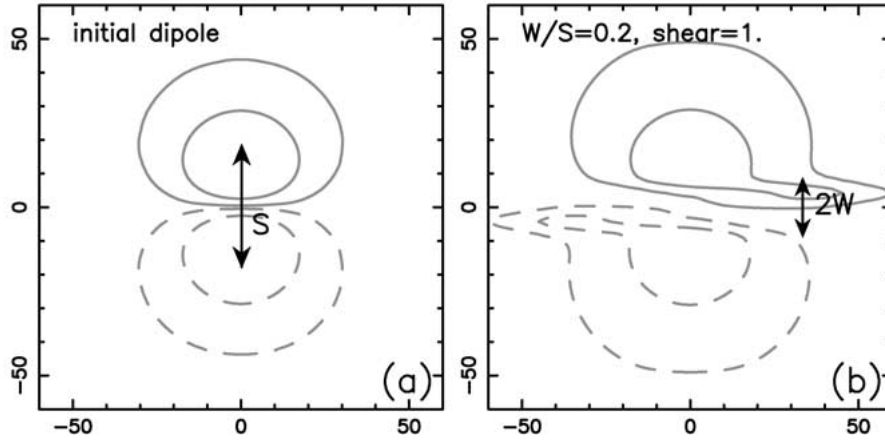


Figure 1. Magnetic field distribution for: (a) the initial bipolar configuration, and (b) after applying a shear concentrated in the vicinity of the PIL (see Equation (13)). Isocontours of positive/negative B_n are drawn with *continuous/dashed lines*.

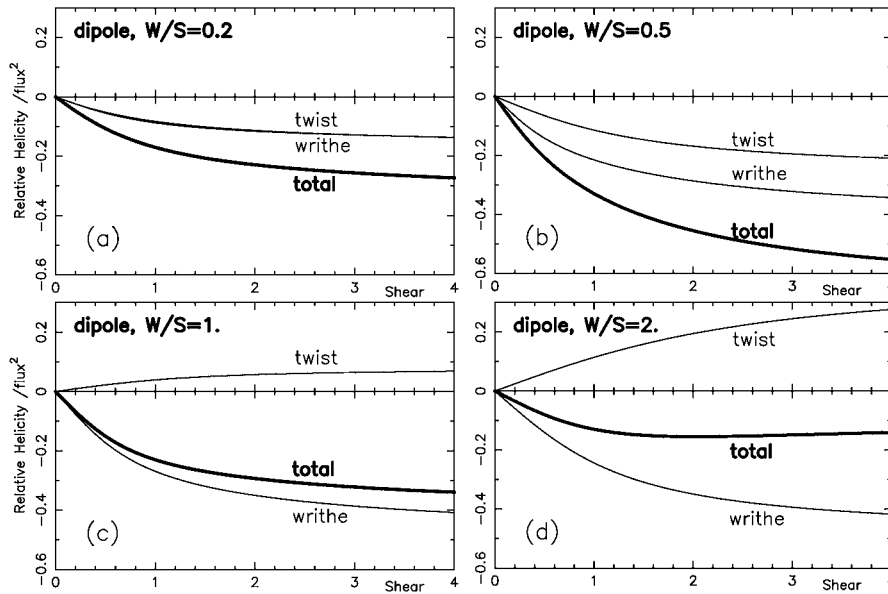


Figure 2. Injection of magnetic helicity by shearing motions in the dipolar configuration of Figure 1 for different extension of the shearing motions the PIL. The abscissa is the shear distance in units of the bipole size S , and the helicity is written in units of Φ^2 (where Φ is the magnetic flux of one polarity). Three quantities are plotted: twist, writhe and total magnetic helicity (see Equation (11)). The total injected helicity is drawn with *thicker lines*.

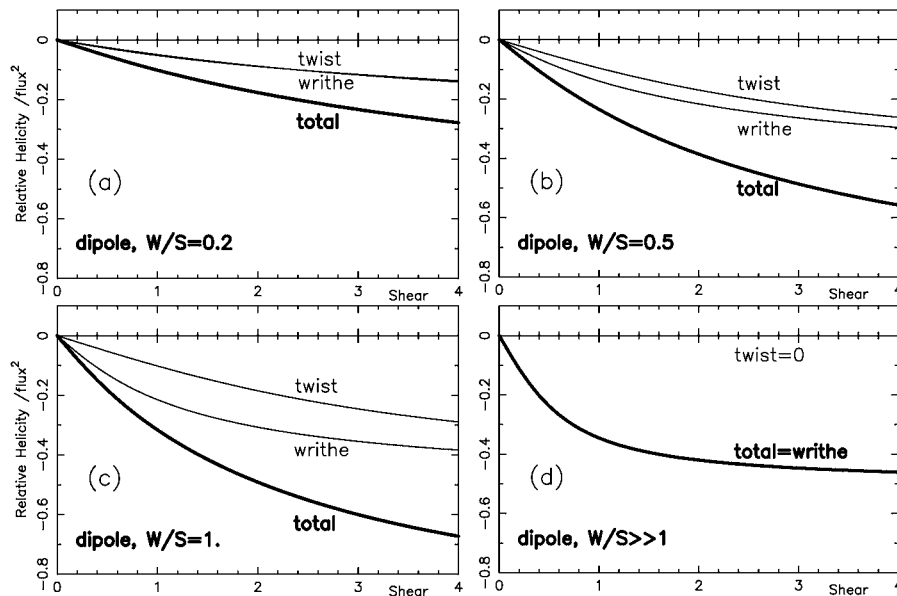


Figure 3. Injection of magnetic helicity by shearing motions in the dipolar configuration of Figure 1(a) for shearing motions decreasing exponentially with the distance to the PIL (Equation (14)). The drawing conventions and the axis extensions are the same as in Figure 2. For such shear profile, the twist helicity has always the same sign as the writhe helicity, and the twist helicity only vanishes in the limit of a very broad shear ($W \gg S$).

The above result (that twist and writhe helicity are nearly the same) is indeed general for shearing motions parallel to the PIL and concentrated around it in symmetric magnetic configurations. This is illustrated in Figure 3(a), where we show the result obtained with the second shear profile, and generalized below. Let us consider one elementary portion of the sheared field located at \mathbf{r}_s (having flux $B_n dS$ say) and two elementary portions of the positive and negative unsheared field (located respectively at \mathbf{r}_P and \mathbf{r}_N (having flux $B'_n dS'$ and $-B'_n dS'$). In the limit $W \ll S$, the rotation rate ($d\theta/dt$, Equation (8)) of $\mathbf{r}_s - \mathbf{r}_P$ is opposite to the rotation rate of $\mathbf{r}_s - \mathbf{r}_N$; this results in an elementary helicity injection which is the same for the writhe and the twist (see Equation (11)).

3.3. COMPETITION BETWEEN WRITHE AND TWIST HELICITY

We analyze below the influence of the width W of the shearing region on the amount of magnetic helicity injected. The amount of flux which is sheared increases with W/S , as does the amount of helicity injected as writhe (Figures 2 and 3). The same is true for the twist helicity for small values of W/S , but, as the sheared region extends, the twist helicity becomes a decreasing function of W/S . This is because the shearing motions rotate, on average, the field located at large $|y|$ in the opposite direction to the field located at small $|y|$. This differential

effect implies that the twist helicity depends on the spatial distribution of the shear while, on the contrary, the writhe helicity is relatively non dependent on it (the shear profile is averaged in the integral associated to the writhe in Equation (11)). In general when the shear is more important close to (resp. away from) the PIL, the twist helicity adds up to (resp. subtracts from) the writhe helicity.

The previous general results are illustrated by the two shearing profiles considered above. For the sinusoidal profile (Equation (13)) $|\Delta H_r|_{\text{twist}}$ is a decreasing function of W/S for $W/S \geq 0.4$. The injection of twist helicity vanishes for $W/S \approx 0.85$, changing in sign for larger values of W/S (Figures 2(c) and 2(d)). For $W/S > 0.85$, the field located at large $|y|$ values is more sheared than the field located at small $|y|$ values, then the shearing motion inputs positive twist. For the exponential profile (Equation (14)), the magnetic field is always more sheared close to the PIL, then the twist helicity has always the same sign as the writhe (Figures 3(b) and 3(c)). It only vanishes in the limit $W \gg S$ (when both magnetic polarities are simply moved along the PIL without deformation).

3.4. TOTAL INJECTION OF MAGNETIC HELICITY

In the case of shearing motions parallel to the PIL, both the writhe and twist helicities increase with W , and they also add up for $W \ll S$. But for large values of W the twist helicity either vanishes or changes in sign. Subsequently, the maximum injected helicity is generally expected when the shear profile affects most of the magnetic flux (so W is of the order of S).

The combined effect of writhe and twist makes the total magnetic helicity maximum for $W/S \approx 0.5$, when considering the sinusoidal profile (keeping the magnetic flux Φ constant). For shear amplitudes (at) smaller than the region size S , the magnitude of the helicity is below $0.3\Phi^2$, while for larger shear amplitudes, this amount is only multiplied by a factor 2 (Figure 2). However, such large shear amplitudes have not been observed (even for the case $at = S$ shown in Figure 1!). For shear profiles having a larger spatial extension W , the amount of helicity injected has a maximum (e.g., Figure 2(d)). For these broader shear profiles, this maximum is lower than $0.15\Phi^2$ ($0.1\Phi^2$ for $W \gg S$).

The exponential profile (Equation (14)) is probably one of the most efficient profiles to inject helicity, because writhe and twist do not subtract. For a given shear amplitude (at) and a given magnetic flux (Φ), the injection of helicity is maximum for $W/S \approx 1.5$. Indeed, around this maximum, the helicity injected depends little on W/S , since for $W/S = 1$ or 2 the value decreases only $\approx 1\%$. The limit of very large shears ($at \gg S$) gives a helicity of Φ^2 (equally distributed between shear and twist). However, for $at \leq S$ the maximum helicity is $0.3\Phi^2$, comparable to the maximum amount injected by the sinusoidal profile.

3.5. HELICITY INPUT IN THE SOLAR CONTEXT

The above estimates are probably generous upper bounds for the helicity injected by photospheric shearing motions for three main reasons. First, the motions are affecting all the magnetic flux around the PIL. Second, the motions are coherent both spatially and temporarily. Finally, the shear amplitude considered (the size of the active region) is a large upper bound. In the solar context, shearing motions are likely to be localized, not necessarily coherent from place to place and moreover time dependent (with changes of direction or even reversals of flows). Each of these effects decreases the amount of helicity injected.

Recently, Chae (2001) and Chae *et al.* (2001) analyzed the magnetic helicity injection in two active regions. They deduced the horizontal flows from MDI/SOHO magnetograms using a local cross correlation tracking technique. The maximum injection of the helicity in both active regions is $3 \times 10^{-3} \Phi^2$ during 27 hours and $3 \times 10^{-2} \Phi^2$ during 50 hours, respectively (Φ is the active region flux, which is around 1.7×10^{21} and 10^{22} Mx, respectively). As expected these values are well below (resp. two and one order of magnitude) the maximum values obtained above in the theoretical cases. The three reasons mentioned above contribute to these lower values. The cancellation of the helicity injected at different locations of the active regions and the time evolution of the flows are more significant. For the second case studied (Chae *et al.*, 2001), the injected helicity rate decreases to a very low value after 2 days, while in the first case (Chae, 2001) the injected helicity rate changes in sign after only 20 hours!

The most significant injection is very likely produced by coherent and long-lasting shearing motions (similar in characteristics to the theoretical profiles analyzed above). These motions, because of their spatial and temporal coherence, should be the most obvious to observe. Presently, this type of motion has not been reported frequently. Moreover, these motions bring only a small amount of helicity, typically of the order of one tenth of Φ^2 . We conclude that shearing motions, which have a spatial scale comparable or lower than an active region, are likely to inject only a relatively small amount of magnetic helicity into the corona.

4. Generation of Magnetic Helicity by Differential Rotation

The main large-scale shearing motion is differential rotation. It is both spatially and temporally coherent, being, therefore, a candidate to inject magnetic helicity into the corona. Some of the results for differential rotation (e.g., the competition between writhe and twist) can be qualitatively deduced from the sinusoidal profile (Equation (13)) in the limit $W \gg S$, but, since differential rotation is a large-scale process independent of the active region properties, this shearing motion is not necessarily parallel to the PIL (as supposed in Section 3). We present below an extended study of the role of differential rotation in providing helicity to the coronal field.

4.1. TWIST AND WRITHE HELICITY FOR DIFFERENTIAL ROTATION

The hypotheses in Sections 2.2 and 2.3 and (horizontal flows and conservation of the vertical magnetic flux at the photospheric level) are well suited to apply our results to differential rotation. We will consider the following classical expression for differential rotation:

$$\omega(L) = a + b \sin^2 L + c \sin^4 L, \quad (15)$$

where L stands for the latitude. Such angular velocity transforms the photospheric flux distribution, injecting helicity into the corona. In the numerical applications below, we will take $a = 14.38 \text{ deg day}^{-1}$, $b = -1.95 \text{ deg day}^{-1}$, $c = -2.17 \text{ deg day}^{-1}$ as given by the cross-correlation analysis of Kitt Peak magnetograms from 1975 to 1991 (Komm, Howard, and Harvey, 1993). These values are very close to the recent ones deduced from seismology measurements with MDI (e.g., Charbonneau *et al.*, 1999, and references therein). It is worth mentioning that very similar results would be obtained with the other values present in the literature (where the variation of b and c is less than 20% of the above values).

Let us use a Cartesian frame, with \hat{x} (respectively \hat{y}) pointing in the east-west (respectively south-north) direction. We further assume for simplicity (and because $\omega(L)$ differs little from a linear profile on the scale size of an AR) a locally linearized form of Equation (15) (see DeVore, 2000). As shown at the end of Section 4.3, this approximation is precise enough. The shear velocity induced by the differential rotation is:

$$\begin{aligned} v_x(\text{diff. rot.}) &= y 2 \sin L \cos^2 L (b + 2c \sin^2 L) \\ &= y \Omega. \end{aligned} \quad (16)$$

Equation (8) then gives:

$$\frac{d\theta}{dt} = -\Omega \sin^2 \theta. \quad (17)$$

Including Equation (17) in Equation (9) gives the injection of relative helicity by differential rotation. We split this expression into two terms:

$$\begin{aligned} \frac{dH_r}{dt}(t) &= \frac{\Omega}{2\pi} \int \int_{B_n B'_n > 0} (\sin^2 \theta) B_n B'_n dS dS' - \\ &\quad - \frac{\Omega}{2\pi} \int \int_{B_n B'_n < 0} (\sin^2 \theta) |B_n B'_n| dS dS' \\ &= \left. \frac{dH_r}{dt}(t) \right|_{\text{twist}} + \left. \frac{dH_r}{dt}(t) \right|_{\text{writhe}}. \end{aligned} \quad (18)$$

With differential rotation both $\Delta H_r|_{\text{twist}}$ and $\Delta H_r|_{\text{writhe}}$ are monotonic functions of time because the signs of $dH_r/dt|_{\text{twist}}$ and $dH_r/dt|_{\text{writhe}}$ are fixed according to

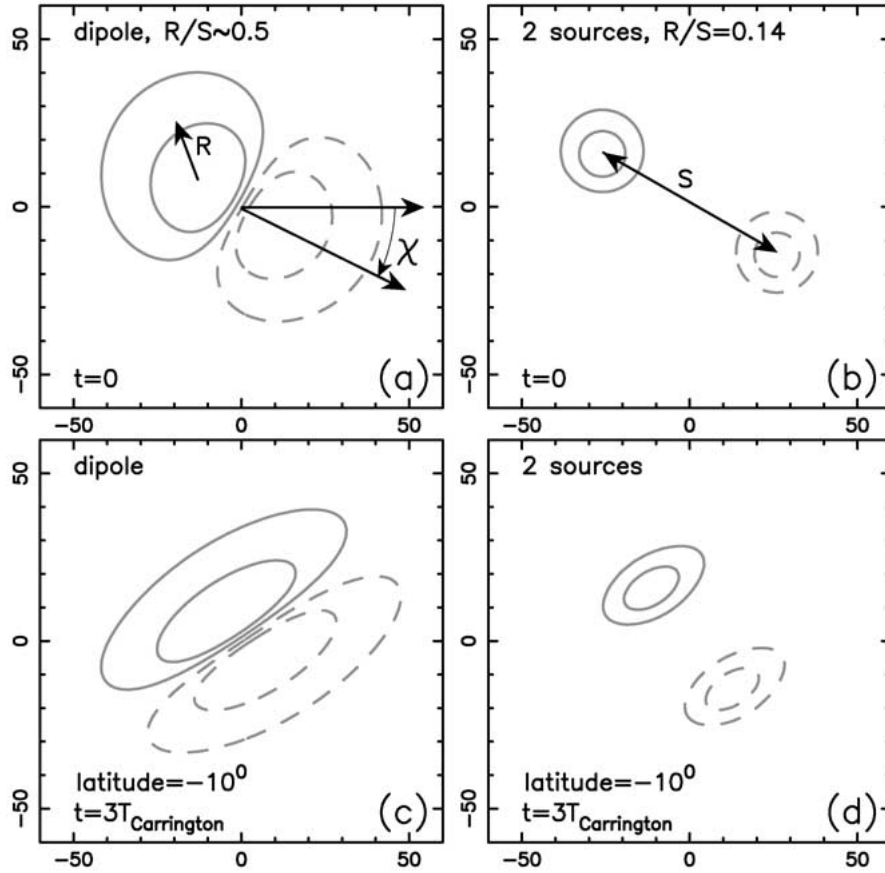


Figure 4. Photospheric magnetic field for two typical theoretical distributions of B_n created by: (a) a subphotospheric horizontal dipole, and (b) two subphotospheric sources (the two distributions are simplified configurations representing, respectively, evolved and young active regions). R is the radius of the polarities, S is the size of the region and χ is the tilt angle. Isocontours of positive/negative B_n are drawn with *continuous/dashed* lines. The *top figures* show the initial field distribution and the *bottom figures* represent the distributions distorted by differential rotation after 3 Carrington rotations (taking a mean latitude of -10°).

the hemispheric location of the AR. However, the generation of helicity by twist and writhe are in competition; they have opposite signs but their magnitudes are similar as it is the case in the previous section for shearing motions with a broad shear profile (Figure 2(d)). This implies that the total helicity ΔH_r is only a fraction of these helicity injections.

4.2. MAGNETIC CONFIGURATIONS ANALYZED

We analyze here two particular magnetic configurations: (a) one created by a subphotospheric horizontal dipole (as in Section 3), and (b) another one created by

two subphotospheric magnetic sources (Figure 4). Configuration (b) converges to configuration (a) when the two sources are infinitely close; (a) is the same configuration used by DeVore (2000) and presents the main characteristics of evolved ARs. In young ARs, the photospheric magnetic field is more concentrated than the distribution of B_n given by the magnetic dipole; in such cases, configuration (b) is more appropriate. These flux distributions are characterized, as in Section 3, by their magnetic flux Φ and their size S . We also define the radii of their polarities as $R_+ = R_- = R = \int_{B_n > 0} |B_n| \sqrt{(\mathbf{r} - \mathbf{r}_+)^2} dS / \Phi$. We study the injection of helicity for various ratios of R/S ($R/S = 0.5$ for the horizontal dipole, $R/S = 0.06, 0.24$, for the magnetic sources). The analytical distributions of B_n are computed on a mesh to simulate magnetograms; that is to say, we build a model magnetogram. The resolution used in Figures 5–7 is 2 Mm in order to represent the resolution of present magnetographs (except for the case $R/S = 0.06$ where it is 1 Mm).

Statistically, the leader polarity of solar ARs is closer to the equator than the following one (Joy’s Law, Hale *et al.*, 1919), though a great dispersion of the tilt is present. The tilt angle χ of the configuration is the angle between the vector $\mathbf{r}_+ - \mathbf{r}_-$ and the solar equator (Figure 4). χ is defined, in the interval $[-90^\circ, 90^\circ]$, symmetrically in both hemispheres; so that positive tilt angles correspond to regions with a leader (or westward) polarity towards the pole (then $\chi > 0$ is in the clockwise, respectively counter clockwise, direction in the southern hemisphere, respectively northern hemisphere). With this convention, the effect of differential rotation is to increase monotonically the tilt angle χ in both hemispheres. We show below that the tilt χ , the latitude L and the magnetic flux Φ are the main parameters determining the amount of magnetic helicity injected by differential rotation.

Active regions are usually more complex than the above simple bipolar configurations; in particular, there are several small parasitic polarities present creating a complex magnetic topology which is determinant for flare physics (e.g., Démoulin *et al.*, 1997). However, these small polarities will have a very small effect on the computation of the injected helicity because of the square of the magnetic flux entering in Equations (11) and (18). This remark does not apply to the more complex cases, e.g., quadrupolar configurations with similar polarity fluxes; in such cases the helicity computations have to be done using Equation (18). It is also worth noting that we are using potential field models only to define the B_n distribution at the photospheric level (model magnetograms), and that we are making no further hypotheses on the chromospheric and coronal magnetic fields.

We are showing in Figures 5–7 the results with a latitude of -10° so that these theoretical plots can be directly compared to the results obtained using observed magnetograms for AR 7978 (Démoulin *et al.*, 2001). The injection time scale ($1/\Omega$) decreases with latitude L for $|L| \leq 35^\circ$ with $c = 0$ and for $|L| \leq 45^\circ$ with Komm, Howard, and Harvey (1993) values, while the maximum injected helicity is nearly unchanged (even with the full differential rotation profile, see below). From Equations (16) and (18), the helicity injection rate is approximately proportional to the latitude L , for $|L| \leq 40^\circ$; therefore, Figures 5–7 can be easily scaled to other

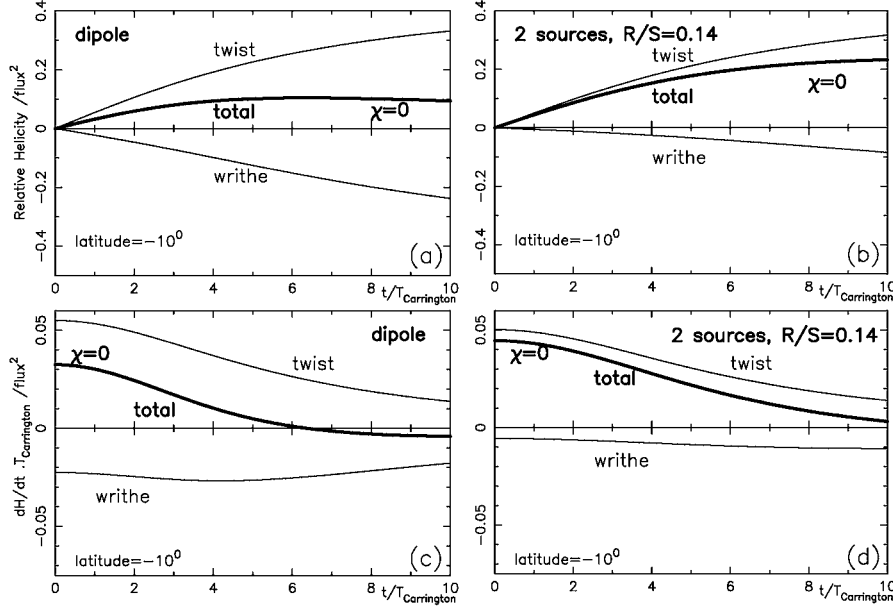


Figure 5. Injection of magnetic helicity by the two typical theoretical distributions of B_n shown in Figure 4. (a, b) Injection of helicity by differential rotation in units of Φ^2 versus time in units of the Carrington period (where Φ is the magnetic flux crossing the photosphere for one polarity). Three quantities are plotted: twist, writhe, and total injection rate of magnetic helicity for an initial tilt $\chi = 0$. The total helicity injected is marked by the *thicker lines*. (c, d) The injection rate of helicity by differential rotation (dH/dt) is normalized by $\Phi^2/T_{\text{Carrington}}$. The curves depend on the same parameters as in (a, b).

latitudes. The choice of a negative latitude lets us also consider a shear profile with the same sign as in Section 3 (compare Figure 1 and Figure 4).

4.3. THE DEPENDENCE OF THE HELICITY INJECTION

4.3.1. Temporal Evolution

For the field of a dipole oriented parallel to the solar equator (tilt angle $\chi = 0$), a little more helicity is injected as twist than as writhe (Figures 5(a) and 5(c)). The total injected helicity is then relatively small and maximum around the 6th rotation for a latitude of $|L| = 10^\circ$. With a more concentrated field, the helicity due to twist is almost the same, but in the case of writhe is much lower (compare right and left columns in Figures 5), then the total helicity is larger and is maximum at longer times.

Our results for dH_r/dt , considering the horizontal dipole with $\chi = 0$ (Figure 5) and with $\chi = 90$ (not shown but similar to the time derivative of the plot shown in Figure 2(d)) agree exactly with those of DeVore (2000) when computed with the same normalization. It is worth remarking that dH_r/dt is computed numerically in a different way in both studies; we are using Equation (18) while DeVore is

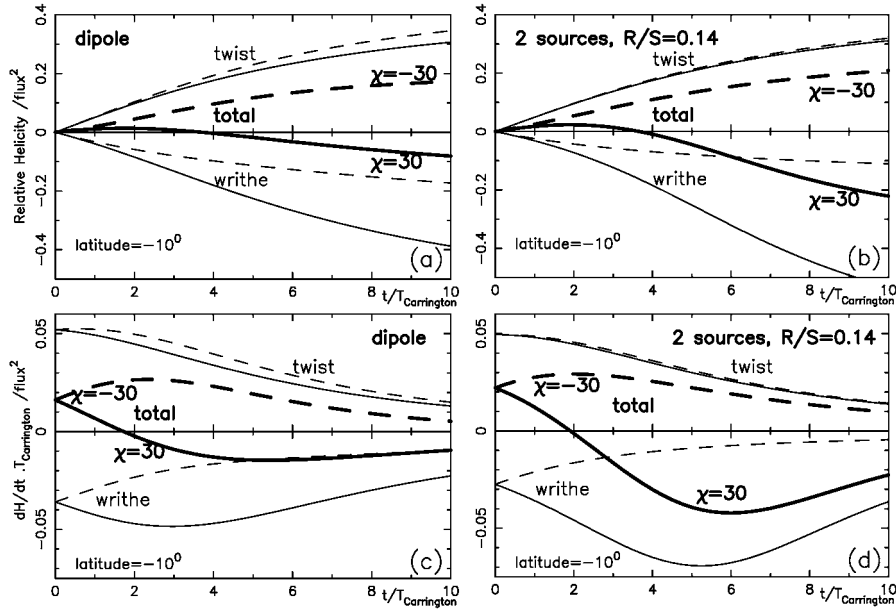


Figure 6. Same as Figure 5 but for an initial tilt $\chi = 30$ (continuous lines) and $\chi = -30$ deg (dashed lines). The total injected helicity is drawn with thicker lines.

rather using Equation (5) and a numerical evaluation of $A_0(t)$ for the instantaneous $B_n(t)$ (see his Equations (3) and (4)). For the helicity H_r , there is also a main difference between the two approaches: DeVore computes H_r from the coronal force-free field, while here H_r is the helicity injected by boundary motions (see Equation (11)).

4.3.2. Tilt Angle

The initial tilt angle χ is the parameter that decides if twist or writhe injection will weakly dominate later on. As an illustrative example we show the case $\chi = \pm 30$ in Figure 6. The case $\chi = -30$ (leader inclined towards the equator) has a total helicity growing with time, while the case $\chi = 30$ starts with a positive injection which rapidly reverses sign (because of a strongly negative writhe injection). Moreover, except close to the initial time, where both injections have the same value, there is no symmetry between $\chi = +30$ and $\chi = -30$.

While the helicity injection is an even function of χ at $t = 0$ (see Equation (21) below), an asymmetry progressively builds up with time; for a very long time the helicity $H_r(\chi)$ is an odd function of χ (Figure 7; note, however, that this is only a theoretical limit since on the Sun several other processes play a dominant role on such long time scales). For the initial tilt interval $[-45^\circ, 45^\circ]$ (bipoles oriented in the east–west direction) and for short shearing times, the injected helicity has the sign of the observed hemispheric dominance (negative/positive helicity in the northern/southern hemisphere; Seehafer, 1990; Pevtsov, Canfield, and Met-

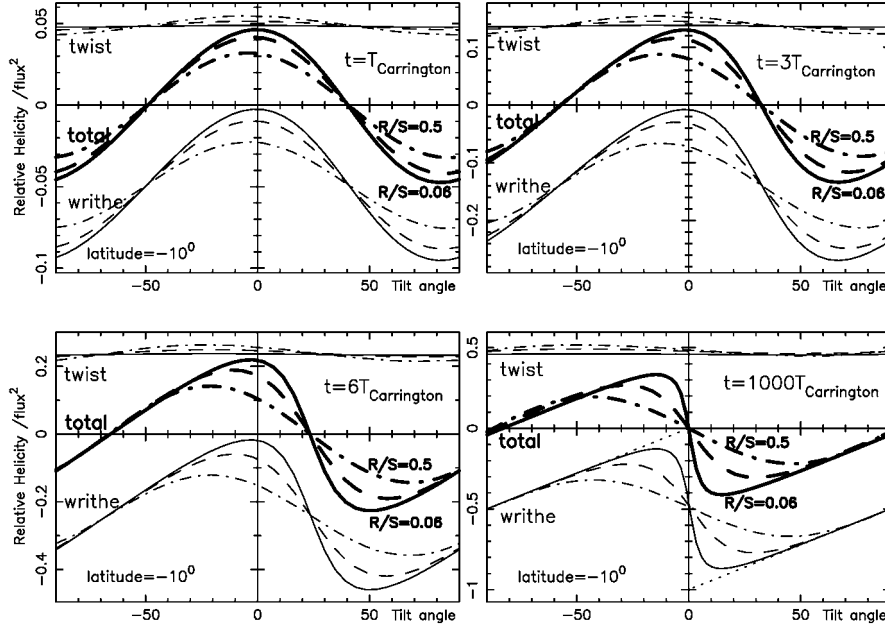


Figure 7. Temporal evolution of the twist, writhe and total magnetic helicity injected by differential rotation as a function of the initial tilt χ of the bipole (bipoles with a positive tilt have a leader which points towards the south pole). Three models are represented, one with a normal field component (B_n) distribution given by a subphotospheric horizontal dipole shown in Figure 4(a) (with a ratio of the polarity radius, R , over the size, S , of the region $R/S \approx 0.5$), and two with B_n given by two subphotospheric sources ($R/S \approx 0.24$, not labeled, and 0.06). The helicity is in units of Φ^2 (where Φ is the magnetic flux of one polarity), note the evolution of the helicity magnitude on the left axis. For small shearing times, H_r is an even function of χ . With time, H_r becomes progressively an odd function of χ . In the figure for $t = 1000 T_{\text{Carrington}}$, which is a pure theoretical limit including only differential rotation (see Appendix A), the analytical limits for very large times ($t \gg T_{\text{Carrington}}$) of Equations (22) and (23) are added (two *straight dash-dotted lines* are plotted in the limit $R/S \rightarrow 0$, so $\chi_l = 0$).

calf, 1995). With time, this interval progressively shifts to $[-90, 0]$ (bipoles which were initially inclined towards the equator). In agreement with the conclusion of DeVore (2000), this behavior is coherent with the observed helicity dominance per hemisphere, since ARs are in average more tilted towards the equator.

The results of Figure 7 can also be understood qualitatively when compared to the results of van Ballegoijen and Martens (1990). These authors consider an initial magnetic configuration formed by a potential arcade invariant by translation. In this simple configuration, the sign of the injected helicity can be deduced from the evolution of the magnetic shear angle (angle between the direction of the arcade field lines (AFL) and the normal to the PIL). Applying the analysis in their Section II to the southern hemisphere, we find a different evolution in the four initial tilt angle χ intervals. In the interval $-90 \leq \chi \leq -45$, the AFL are initially more south-north oriented, so more affected by differential rotation than the PIL.

This implies a negative shear angle, so a negative helicity input. This tendency reverses when the PIL becomes more oriented in the south–north direction than the AFL and, both, shear angle and magnetic helicity reverse in sign (Figure 7). In the interval $-45 \leq \chi \leq 0$, the AFL are always more east–west oriented than the PIL. This results in a shear angle and a magnetic helicity which are always positive. A similar analysis of the shear angle evolution shows that the magnetic helicity is first positive, then negative in the interval $0 \leq \chi \leq 45$, while it stays negative in the interval $45 \leq \chi \leq 90$.

4.3.3. *Relative Extension of the Photospheric Polarities*

The helicity injection is affected by the photospheric B_n distribution. The relative extension of the polarities can be characterized by the ratio between the radius of the polarities, R , and the size of the AR, S . The total injection of helicity is less efficient when the magnetic polarities are more extended, so for large R/S (compare the left and right columns of Figures 5 and 6 as well as the curves in Figure 7).

The dependence of the helicity on R/S comes mainly from the writhe term. To understand this it is worth remembering that the helicity injection related to the pair $(B_n \, dS, B'_n \, dS')$, located at $(\mathbf{r}, \mathbf{r}')$, depends on $\sin^2 \theta$ (Equation (18)). For small relative extension of the polarities all pairs have similar orientation angles θ , and so their contributions add up $(dH_r/dt(\chi))|_{\text{writhe}} \approx \Omega \Phi^2 / \pi \sin^2 \chi$. This results in a strong dependence on the tilt angle. The spread of $\sin^2 \theta$ increases with R/S ; then, the modulation of the writhe helicity with χ around a mean value becomes less important (Figure 7). The relative extension of the polarities (R/S) has a small effect on the twist injection (the low χ dependence present in Figure 7 comes from the fact that the polarity is no longer circular when R is comparable to S). The combination of these two effects gives a total helicity which can be a factor 2 larger in a young AR (concentrated field) than in an evolved AR (closer to the dipole case).

4.3.4. *Full Differential Rotation Profile*

In general, the extension of an AR is small compared to the solar radius. This implies that the linearized differential profile used above is expected to give a good approximation of the injected helicity. Indeed, the quasi-cancellation of twist and writhe helicity makes this approximation even better. The linearized expression for the differential rotation profile (Equation (16)) gives a total helicity injection having a 10% difference with the injection obtained using the full differential rotation profile (Equation (15)) in the case of an AR at a latitude of 10° and extending $\pm 10^\circ$ in the north–south direction. This estimate is indeed an upper bound since the difference decreases with a larger mean latitude as the profile of differential rotation is less curved.

4.4. INITIAL INJECTION OF MAGNETIC HELICITY

The above numerical results show that an important parameter for the injection of helicity is the tilt angle χ . We extend below this result to more general configurations and we obtain analytical results for the initial injection.

In order to analyze only the effect of the tilt angle χ , let us consider the same magnetic configuration but tilted at variable angles χ . Let us restrict the analysis to an initial B_n distribution which has a mirror symmetry with respect to the axis joining the mean positions of negative and positive polarities (the axis joining the points defined above by \mathbf{r}_+ and \mathbf{r}_-). With this hypothesis on the initial field distribution, the initial injection of writhe for a given tilt angle χ is simply related to the injection obtained with an east–west orientation ($\chi = 0$):

$$\left. \frac{dH_r}{dt}(\chi) \right|_{\text{writhe}} = \cos 2\chi \left. \frac{dH_r}{dt}(0) \right|_{\text{writhe}} - \frac{\Omega\Phi^2}{\pi} \sin^2 \chi, \quad (19)$$

where Φ is the magnetic flux crossing the photosphere in both polarities.

Similar considerations apply to the twist injection:

$$\left. \frac{dH_r}{dt}(\chi) \right|_{\text{twist}} = \cos 2\chi \left. \frac{dH_r}{dt}(0) \right|_{\text{twist}} + \frac{\Omega\Phi^2}{\pi} \sin^2 \chi, \quad (20)$$

the main difference being the sign in front of the last term.

Equations (19) and (20) show how the initial helicity injection changes with the tilt of the AR with respect to the east–west direction. In particular, for $\chi = \pm 45^\circ$ both the writhe and twist injections depend only on the differential rotation profile (via Ω) and on the total magnetic flux, but not on the precise distribution of the flux. Moreover, for these values of χ , the writhe and the twist injection cancel exactly, so that there is no net injection of magnetic helicity.

These results apply, in particular, to a dipole distribution as the one considered by DeVore (2000) and to the configurations studied above. Furthermore, they generalize the results for a dipole to flux distributions which have a mirror symmetry. Adding Equations (19) and (20) one gets

$$\frac{dH_r}{dt}(\chi) = \cos 2\chi \frac{dH_r}{dt}(0). \quad (21)$$

This implies that the initial injection of helicity is an even function of the tilt χ (Figure 6). Later on, this symmetry is broken (Figure 7). Though here we use a B_n photospheric distribution that has a mirror symmetry, the previous results are expected to be a good approximation to solar ARs because dH_r/dt is an integral quantity little affected by the precise distribution of the flux. These analytical results can be used to obtain an estimation of the injection rate in a bipolar AR.

5. Comparison with Twisted Flux Tubes

In order to see how large the amount of helicity injected by shearing motions is, it is worth comparing it to the helicity present in a twisted flux tube. The magnetic helicity contained in a twisted flux tube having N turns and a magnetic flux Φ_t is simply $N\Phi_t^2$ (Berger, 1984).

The localized shearing motions analyzed in Section 3 can be compared to the emergence of a twisted flux tube having the same magnetic flux as that in the sheared region ($|y| \leq W$). Let us call Φ_W the total positive sheared flux and, as above, Φ the total positive flux, then write the injected helicity as $c\Phi\Phi_W$. For small W/S values, $|c|$ is an increasing function of the shear amplitude (at) but it is a decreasing function of the shear spatial extension (W/S). The limit $at \gg S$ and $W \ll S$ provides an upper-bound to $|c|$. This limit is obtained analytically with an analysis similar to the one done in Appendix A; it gives a helicity injection of $2\Phi\Phi_W$. For a shear amplitude equal to the region size ($at = S$), a numerical integration of Equation (11) shows that this injection is about half the above limit. Such an amount of helicity, $\approx \Phi\Phi_W$, can be comparable, or even larger for $\Phi_W \ll \Phi$, to the magnetic helicity, $N\Phi_W^2$, which can be carried by a small-scale emergence of a twisted flux tube.

However, for $W \ll S$, so $\Phi_W \ll \Phi$, the shear motions bring a relatively small quantity of magnetic helicity to the whole magnetic configuration as follows. Coronal magnetic configurations with S-shaped X-ray loops are routinely observed with *Yohkoh* and are frequently associated with coronal mass ejections (e.g., Canfield, Hudson, and McKenzie, 1999; Glover *et al.*, 2000). An important fraction of these sigmoid structures are interpreted as being twisted magnetic flux tubes with a twist of the order of one turn (e.g., Rust and Kumar, 1996; Titov and Démoulin, 1999; Portier-Foazzani *et al.*, 2001). The magnetic helicity of these coronal configurations is then of the order of Φ^2 . This is above the maximum helicity ($\approx 0.3\Phi^2$) that shearing motions can inject for a shear amplitude of S (a large shear upper bound from the observed photospheric magnetic field distributions!). The typical amount of helicity injected by shearing motions is rather of the order of $0.1\Phi^2$ (and even lower for less organized shearing motions, see Section 3.5), so it is at least one order of magnitude less than what is required to explain the observed coronal sigmoids.

The same conclusion is reached for the differential rotation as follows. The maximum amount of helicity injected by differential rotation for an AR at a latitude of $|L| = 10^\circ$ after three Carrington rotations is $\approx 0.1\Phi^2$ if the field is concentrated (at $|L| = 30^\circ$, that amount is achieved after one Carrington rotation). Later on, the AR becomes less concentrated, and a dipole better represents the photospheric field distribution. At that point, the maximum amount of helicity is found to be $\approx 0.2\Phi^2$ (Figure 7) for very long shearing times. Indeed, a twist of 0.2 turns in any coronal magnetic configuration is almost not observable because magnetic configurations are far from being simple straight flux tubes with simple photospheric field distri-

bution, and because only few coronal loops with the right projection can be seen at a given time.

Finally, we recall that a significant twist is needed to keep the coherence of magnetic flux tubes as they travel through the convective zone (e.g., Emonet and Moreno-Insertis, 1998). These flux tubes, which form active regions after crossing the photosphere, are then expected to carry a significant amount of magnetic helicity (of the order of few Φ^2). We think that they are the main candidate to explain the origin of the coronal magnetic helicity.

6. Conclusion

We estimate the amount of magnetic helicity that can be injected into the corona by horizontal photospheric motions. Following the theoretical work of M. A. Berger (see references in the previous sections), we have extended C. R. DeVore's computation so that the helicity injected into the corona can be computed for any distribution of the magnetic field at the photosphere, so from any observed magnetogram (Section 2.2). We then separate the helicity injection into two terms: twist (intrinsic rotation of photospheric polarities of a given sign) and writhe (relative rotation of opposite polarities).

For shearing motions concentrated in the vicinity of the photospheric inversion line (PIL) of the vertical field component (B_n), both twist and writhe helicity add up. Then, in this case, the amount of coronal helicity increases monotonically with the shear amplitude until it saturates for very large shear amplitudes. This saturation is due to both the finite rotation of each polarity (twist) and the finite rotation of positive and negative polarities (writhe) in the limit of a large shear (maximum rotation of $\frac{1}{2}$ of turn in each case). However, when the sheared region is more extended around the PIL, the sheared regions farthest from the PIL inject an opposite twist, so that the magnetic helicity injected decreases with a larger extension of the sheared region. When the shear velocity is increasing with the distance to the PIL, the twist and writhe helicity injected have opposite signs, and then, they compete. In such cases the amount of coronal helicity reaches a maximum after a finite shear, then declines and even changes in sign for a larger shear (Section 3).

A well observed example of such large-scale shear is differential rotation (Section 4). The helicity injected into a bipolar AR depends mainly on the following five parameters: the temporal duration of the shearing motions, the AR latitude L , the AR magnetic flux Φ , the AR tilt χ (inclination of the bipole with respect to the solar equator) and the ratio R/S of the mean polarity size over the AR size. We fully confirm, using a different numerical computation method, the results found by DeVore (2000) about the amount of helicity injected by differential rotation for the two cases he studied (an initial magnetic dipole with a tilt $\chi = 0$ and 90°). Analytical limits for the initial injection rate (Section 4.4) and for very long

shearing periods (Appendix A) have been found. They are successfully used to test the numerical computations.

We have determined the amount of helicity injected as a function of the five parameters mentioned above. Because the evolution with time of the helicity is generally non-monotonic, individual results, such as those in Figures 5–7 are needed to analyze particular cases for a given interval of time. However, some general results can be summarized as follows. The injection of magnetic helicity is nearly proportional to the latitude L for the range of latitudes where ARs are observed. The injected helicity is simply proportional to Φ^2 . The initial injection has a $\cos 2\chi$ dependence, giving a negative/positive injection in the northern/southern hemisphere for ARs more inclined in the east–west direction. This even dependence with χ progressively changes to an odd dependence with χ as the shear amplitude increases (in agreement with van Ballegoijen and Martens, 1990). Finally, the amount of generated helicity depends only slightly on the relative extension of the polarities with respect to the active region size (ratio R/S). A more efficient helicity generation is found for more concentrated fields, so for young ARs (up to a factor 2).

From the analysis of a set of theoretical shearing motions, but also from the inspection of the general formulae, we conclude that the maximum amount of magnetic helicity that shearing motions can provide to the corona is small compared to the magnetic helicity present into a twisted flux tube with significant twist (of the order of one). Most of the observed photospheric motions are likely to be less extended and/or less coherent both in space and time than the studied theoretical motions, and so they bring a lower amount of magnetic helicity. This is indeed the case for motions observed so far (Chae, 2001; Chae *et al.*, 2001). The most efficient shearing motions are affecting a significant part of the flux, in a coherent and systematic way; then such motions, if present, are likely to be easily detected. The only well-known motion of this type is differential rotation. However, we again show that it is not an efficient process to inject a significant amount of magnetic helicity into the corona.

The above results are guide lines for studying the injection of magnetic helicity in active regions. More precise results on particular active regions can be obtained by using directly Equation (11) with observed magnetograms. Because magnetic helicity is well preserved, even in presence of magnetic reconnection, it is a useful physical quantity to follow the evolution of magnetic fields from the convective zone, to the corona, and then to the interplanetary space. This will be the object of the next papers (Démoulin *et al.*, 2001; Green *et al.*, 2002) in the context of coronal mass ejections. One final goal is to determine if the accumulation of magnetic helicity into the corona is at the origin of the coronal mass ejections (Low, 1996).

Acknowledgements

We thank the anonymous referee for his/her positive comments that have contributed to generalize the results of this paper. We thank C. R. DeVore for useful discussions. P.D., C.H.M., and M.C.L.F. acknowledge financial support from ECOS (France) and SETCIP (Argentina) through their cooperative science program (A97U01). L.v.D.G. is supported by the Hungarian Government grants OTKA T-026165, T-032846. P.D. and L.v.D.G. acknowledge the Hungarian-French S&T cooperative program. L.v.D.G. is supported by Research Fellowship F/01/004 of the K.U. Leuven.

Appendix

Injection after a Long Shearing Period

It is instructive to compute analytically the limit, $\lim_{t \rightarrow \infty} \Delta H_r(t)$. First, it illustrates the geometrical interpretation of the injection of helicity in the simple case implying the complete rotation of the polarities. Second, it allows testing the numerical computation of ΔH_r from Equation (11) in the extreme limit when the initial flux distribution is very distorted, probably the worst case concerning the numerical precision. Finally, together with the initial injection rate, it gives some insight on the dependence of ΔH_r with the tilt angle χ . It is worth emphasizing that this limit is purely theoretical since ARs become dispersed after 5 to 8 months and are no longer distinguishable from the network field. On such long time scales other mechanisms such as: magnetic field cancellation, diffusion and meridional flows have to be taken into account. As in Section 4.4, we consider separately the injection of helicity by twist and writhe.

The injection of writhe depends on the relative rotation of the polarities around each other. Let's recall that the axis going through the mean polarity positions (defined by \mathbf{r}_+ and \mathbf{r}_-) is tilted by an angle χ with respect to the equator, that R is the radius of the polarities and that S is the distance separating the polarities. For magnetic polarities limited to a finite extension, $\approx R$, and less extended than their mutual separation ($R \ll S$), there is a tilt angle χ_l so that for $|\chi| > \chi_l$ all the positive flux has no common latitude with the negative flux (e.g., $\chi \approx \chi_l$ in Figure 4(b)). In such a case, the differential rotation can bring the more poleward polarity fully backward (or eastward) from the other one. A simple analytical expression of the writhe helicity can be derived in this case. As in Section 4.4, let us restrict the analysis to an initial B_n distribution which has a mirror symmetry with respect to the axis defined by \mathbf{r}_+ and \mathbf{r}_- . For a bipole tilted towards the pole with $\chi \geq \chi_l$, any vector $\mathbf{r} - \mathbf{r}'$ and its symmetric one will rotate on average, in the limit $t \rightarrow \infty$, by an angle $\pi - \chi$. For a bipole tilted towards the equator with $\chi \leq -\chi_l$ the same analysis gives a mean rotation of $-\chi$. From Equation (11), the injection of writhe helicity is

$$\lim_{t \rightarrow \infty} \Delta H_r|_{\text{writhe}} = -\text{sign}(\Omega) \left(1 - \frac{\chi}{\pi}\right) \Phi^2 \quad \text{for } \chi_l \leq \chi \leq \pi/2, \quad (22)$$

$$\lim_{t \rightarrow \infty} \Delta H_r|_{\text{writhe}} = \text{sign}(\Omega) \frac{\chi}{\pi} \Phi^2 \quad \text{for } -\pi/2 \leq \chi \leq -\chi_l, \quad (23)$$

where Φ is the magnetic flux of B_n for one polarity. For round magnetic polarities limited to a radius R and separated by S , the limit case for $\chi = \chi_l$ is given by

$$\sin \chi_l = 2R/S. \quad (24)$$

On the other hand, for low tilt ($|\chi| < \chi_l$), the injected writhe helicity decreases (only part of the leading, i.e., initially more westward, polarity is rotated to the east of the other polarity). For example, if $\chi = 0$ initially, only half of the leading polarity will be able to move to the east (rotating by 180°) while the other half will stay in front. In this case,

$$\lim_{t \rightarrow \infty} \Delta H_r|_{\text{writhe}}(\chi = 0) = -\text{sign}(\Omega) \Phi^2/2, \quad (25)$$

just the average of Equation (22) and Equation (23) results, if taken for $\chi = 0$. These results have been found numerically for the dipole and source configurations in the limit of a long shearing period (see Figure 7 for $t = 1000 T_{\text{Carrington}}$). In these examples non-zero values of B_n are present indeed in all the ‘photospheric’ plane, but the low field regions have a negligible contribution to the helicity. As expected from Equation (24), the range for the tilt angle $[-\chi_l, \chi_l]$ decreases with the ratio R/S (see Figure 7). These results show that, even when the shear is very large, the writhe helicity is numerically computed with high enough precision.

Next, we analyze the injection of twist helicity. Let us consider a polarity which has initially ($t = 0$) a mirror symmetry with respect to south–north axis (parallel to \hat{u}_y), and let us compute the total $\Delta H_r|_{\text{twist}}$ injected in the limit $t \rightarrow \infty$. Any vector $\mathbf{R} = \mathbf{r} - \mathbf{r}'$ will rotate at this limit by an angle $\pi - \gamma$, where γ is the initial orientation of \mathbf{R} with respect to the east–west direction ($\gamma = \cos^{-1} \hat{u}_x \cdot \mathbf{R}/R$). The symmetric of \mathbf{R} , \mathbf{R}_s , with respect to south–north axis will rotate by γ , i.e. the average rotation of \mathbf{R} and \mathbf{R}_s is 90° . So, a polarity which has initially a mirror symmetry with respect to the north–south axis is rotated up to one fourth of a turn by the differential rotation. It results from Equation (11) that the twist helicity injection for both polarities is

$$\lim_{t \rightarrow \infty} \Delta H_r|_{\text{twist}} = \text{sign}(\Omega) \frac{\Phi^2}{2}. \quad (26)$$

The numerical results (see Figure 7 for $t = 1000 T_{\text{Carrington}}$) are close to this value. It is noteworthy that the mirror symmetry supposed above is only strictly true for the studied configurations (bipole and 2 sources) when $\chi = \pm 90^\circ$. The remaining slight difference between the expected and numerical values comes from the finite discretisation (which is selected to represent the spatial resolution of observations).

The discretisation error is stronger in the direction of vectors $\mathbf{r} - \mathbf{r}'$ when they are inside a given polarity, so the error is larger for the twist than for the writhe. This test has been done on a very deformed model magnetogram and so it is expected to provide a large over-estimation of the discretisation errors present for the injection of helicity during a few Carrington rotations.

References

- Berger, M. A.: 1984, *Geophys. Astrophys. Fluid. Dyn.* **30**, 79.
 Berger, M. A.: 1986, *Geophys. Astrophys. Fluid. Dyn.* **34**, 265.
 Berger, M. A.: 1988, *Astron. Astrophys.* **201**, 355.
 Berger, M. A. and Field, G. B.: 1984, *J. Fluid. Mech* **147**, 133.
 Berger, M. A. and Ruzmaikin, A.: 2000, *J. Geophys. Res.* **105**, 10481.
 Biskamp, D.: 1993, *Nonlinear Magnetohydrodynamics*, Cambridge University Press, Cambridge.
 Canfield, R. C., Hudson, H. S. and, McKenzie, D. E.: 1999, *Geophys. Res. Lett.* **26**, 627.
 Chae, J.: 2001, *Astrophys. J.* **560**, L95.
 Chae, J., Wang, H., Goode, P. R., Strous, L., and Yun, H. S.: 2001, *Astrophys. J.* **560**, 476.
 Charbonneau, P., Christensen-Dalsgaard, J., Henning, R., Larsen, R. M., Schou, J., Thompson, M. J., and Tomczyk, S.: 1999, *Astrophys. J.* **527**, 445.
 Démoulin, P., Bagalá, L. G., Mandrini, C. H., Hénoux, J. C., and Rovira M. G.: 1997, *Astron. Astrophys.* **527**, 305.
 Démoulin, P., Mandrini, C. H., van Driel-Gesztelyi, L. *et al.*: 2001, *Astron. Astrophys.*, in press.
 DeVore, C. R.: 2000, *Astrophys. J.* **539**, 944.
 DeVore, C. R. and Antiochos, S. K.: 2000, *Astrophys. J.* **539**, 954.
 Emonet, T. and Moreno-Insertis, F.: 1998, *Astrophys. J.* **492**, 804.
 Finn, J. H. and Antonsen, T. M.: 1985, *Comm. Plasma Phys. Contr. Fusion*, **9**, 111.
 Glover, A., Ranns, N. D. R., Harra, L. K., and Culhane, J. L.: 2000, *Geophys. Res. Lett.* **27**, 2161.
 Green, L. M., López Fuentes, M. C., Mandrini, C. H., Démoulin, P., van Driel-Gesztelyi, L., and Culhane, J. L.: 2002, *Solar Phys.*, in press.
 Hale, G. E., Ellerman, F., Nicholson, S. B., and Joy, A. H.: 1919, *Astrophys. J.* **49**, 153.
 Komm, R. W., Howard, R. F., and Harvey, J. W.: 1993, *Solar Phys.* **143**, 19.
 Leka, K. D., Canfield, R. C., McClymont, A. N., and van Driel-Gesztelyi, L.: 1996, *Astrophys. J.* **462**, 547.
 Low, B. C.: 1996, *Solar Phys.* **167**, 217.
 Mikić, Z. and Linker, J. A.: 1994, *Astrophys. J.* **430**, 898.
 Pevtsov, A. A., Canfield, R. C., and Metcalf, T. R.: 1995, *Astrophys. J.* **440**, L109.
 Portier-Fozzani F., Aschwanden M., Démoulin P., Neupert W., and EIT Team: 2001, *Solar Phys.* **203**, 289.
 Rust, D. M. and Kumar, A.: 1996, *Astrophys. J.* **464**, L199.
 Seehafer, N.: 1990, *Solar Phys.* **125**, 219.
 Taylor, J. B.: 1974, *Phys. Rev. Lett.* **33**, 1139.
 Titov, V. S. and Démoulin, P.: 1999, *Astron. Astrophys.* **351**, 707.
 van Ballegoijen, A. A. and Martens, P. C. H.: 1990, *Astrophys. J.* **361**, 283.
 Wang, J.: 1996, *Solar Phys.* **163**, 319.